Available online at www.sciencedirect.com
SCIENCE DIRECT
Journal of Sound and Vibration 297 (2006) 72–88
JOURNAL OF SOUND AND VIBRATION
www.elsevier.com/locate/jsvi

Modal characteristics of a simplified brake rotor model using semi-analytical Rayleigh–Ritz method

F. Zhang, L. Cheng*, L.H. Yam, L.M. Zhou

Department of Mechanical Engineering, The Hong Kong Polytechnic University, Hong Kong

Received 22 July 2005; received in revised form 16 January 2006; accepted 16 March 2006
Available online 6 June 2006

Abstract

Emphasis of this paper is given to the modal characteristics of a brake rotor which is utilized in automotive disc brake system. The brake rotor is modeled as a combined structure comprising an annular plate connected to a segment of cylindrical shell by distributed artificial springs. Modal analysis shows the existence of three types of modes for the combined structure, depending on the involvement of each substructure. A decomposition technique is proposed, allowing each mode of the combined structure to be decomposed into a linear combination of the individual substructure modes. It is shown that the decomposition coefficients provide a direct and systematic means to carry out modal classification and quantification.

1. Introduction

Brake squeal is a very notorious noise phenomenon which occurs during the process of vehicle braking [1–3]. Early studies on brake squeal problems can be traced back to 1950s. Even now, consentaneous explanation of such phenomenon still evades researchers due to its fugitive nature and the complex physical interactions between different components involved in a brake system, among which the brake rotor is the most crucial one.

In the generation of brake squeal, the brake rotor reveals its significance mainly in two aspects: the indispensable involvement in the process of friction interaction and the effective sound radiation due to its vibration. Based on a common belief that the brake noise is aroused primarily by the self-excited vibration of the brake structure [1,2], a significant portion of the existing works focuses on structural vibration instead of noise itself.

Commonly used modeling methods for brake systems can be roughly classified into two categories: methods based on analytical continuum theories and the finite element (FE) models. The apparent advantage of FE method rests in its capacity of dealing with more realistic brake rotor models and generating accurate solutions. Both free and forced vibration analyses can be carried out using commercial FE software [4–6]. Systematic methodologies have also been developed to extract structural parameters from FE analysis and

*Corresponding author. Tel.: +852 2766 6769; fax: +852 2365 4703.
E-mail address: mmcheng@polyu.edu.hk (L. Cheng).

0022-460X/$ - see front matter © 2006 Elsevier Ltd. All rights reserved.
doi:10.1016/j.jsv.2006.03.040

then perform stability analysis externally [5]. However, most FE models used for vibration analyses of brake rotor are highly computationally demanding. By contrast, a simplification of the brake system model makes it possible to use more conventional, efficient and physical methods based on analytical continuum theories. Differences in existing models root in different beliefs on the brake noise generation mechanism. Analyses based on such simplified analytical models are able to focus on specific physical aspects and explore major underlying physics of the system. While using analytical continuum models, researchers generally cover only the brake pads and the brake rotor. Such analyses usually focus on the structure interaction and/or modal coupling between the pads and the rotor due to the friction interaction. For example, Ouyang and Mottershead [6,7] proposed a brake model comprising a uniform annular plate and, on the top of it, a rotating mass–damper–spring exciter. Their studies focused on the stability analysis of this parametric excited system. In Húlten et al. [8,9], both the rotor and brake pads were modeled as beam structures. It was proposed that the bending moment of the rotor is responsible for the modal coupling and wave propagation within the rotor.

It is known that a brake rotor responds differently in low- and high-frequency brake squeal [2]. In the case of the low-frequency squeal, the brake rotor is predominated by bending modes without nodal circle. While in the case of high-frequency squeal, the rotor displays both in-plane movement and bending. Controversial viewpoints about the rotor behavior in the high-frequency squeal still exist. Chen et al. [10] claimed that high-frequency brake squeal resulted from modal coupling between an in-plane mode and an out-of-plane (bending) mode of the brake rotor. Therefore, when the in-plane modes of a rotor had the same resonant frequencies with the out-of-plane modes, the in-plane vibration energy was effectively transferred to the out-of-plane vibration that was efficient/sufficient to generate squeal noise. Usually, the out-of-plane mode with a higher resonant frequency adjacent to the in-plane mode tended to be the one that had the same vibration pattern as the squeal deformation shape. However, experiment results reported in a recent paper [11] seem to indicate that frequency lineup of in-plane circumferential (IPC) mode and out-of-plane diametric (OPD) mode had no impact on squeal, which challenged the conventional assumption based on the IPC–OPD frequency coupling. Despite these differences in the interpretation of squeal noise generation mechanism, there is one argument which seems to be well accepted, i.e., a thorough understanding of the structural modal characteristics of the brake rotor is indispensable and critical to further disclose the brake vibration/noise mechanism.

Except FE models, a large majority of analytical models reported in the literature simplified the brake rotor as a uniform annular plate. Although such a model greatly simplifies the mathematical treatment, it inevitably deviates from the real brake rotor structure, since the in-plane and transversal motions are totally decoupled in an annular plate. A more reasonable model should at least consider the practical brake rotor as a combined structure, including a top annular plate connected to a short segment of cylindrical shell. In practice, the existence of the shell segment serves as a vehicle for the coupling between the in-plane and transversal motions of the disc. The degree of difficulty in handling such a model, however, significantly increases. Of a few available references dealing with such models, Bae and Wickert [12] used FE analysis to investigate a disc-hat structure of the brake rotor, which evolves from a simple thin plate with an increasing hat depth. Parametric studies have also been carried out in their paper.

This paper proposes an alternative to the existing FE model using a combined structure, comprising an annular plate connected to a short segment of shell, to model the brake rotor. Artificial springs are utilized to combine them together. The primary aim of the paper is to discuss the modal characteristics of such combined structure using a semi-analytical approach. A numerical procedure for modal analysis is derived by means of Rayleigh–Ritz method. Accuracy of the model is then verified by comparison with FE simulations. Structural coupling phenomena between different parts of the brake rotor are identified through numerical results. Structural modes are investigated and classified according to their deformation features. Emphasis is put on those modes which show strong coupling between the out-of-plane motion of the plate and the in-plane motion of the whole structure. Influences of the rotor dimension are also investigated. It is demonstrated that modal characteristics of the combined structure can be quantitatively evaluated through a decomposition analysis, in which each mode is expanded as a linear combination of individual substructure modes. The linear combination coefficients quantify the contribution of each single

substructure mode to the coupled mode of the combined structure, thus indicating its characteristic deformation pattern.

2. Numerical procedure based on a three-dimensional elasticity theory

The proposed model for a brake rotor comprises an annular plate and a segment of cylindrical shell connected by distributed artificial springs, as illustrated in Fig. 1. Theses springs, having translational stiffness k_u, k_v and k_2, are used to couple the translational deformations in the radial, circumferential and axial directions, respectively, at the interface between the plate and the shell. Meanwhile, rotational springs having distributed stiffness C_2 are also used to couple the bending deformation between the two substructures. Advantages of using an artificial spring system to deal with mechanically coupled structures have been extensively documented in the past. Typical examples can be found in Refs. [13,14], in which artificial springs were successfully applied to a thin cylindrical shell ended with circular plates.

The boundary conditions of the combined structure are implemented in two ways in the present case. One is through the choice of appropriate expansion functions for different displacement components to satisfy certain types of geometrical boundary conditions related to the deformation. This will be clarified in the following sections. The other alternative is again to use artificial springs to impose mechanical constraints, such leading to certain types of boundary conditions. In practice, the brake rotor is screw-mounted on the wheel knuckle through an internal annular plate at the free end of the combined model. To better reflect the reality, additional axial translational springs k_1 and rotational springs C_1 are further incorporated into the model at the free end of the shell segment to impose constrains on the axial translation and bending of the shell.

Various elasticity theories are available in particular for plate or shell structures. For instance, Mindlin plate theory is quite appropriate for the mid-thin plate, and Flügge theory is able to give satisfactory results for the thin but at least moderately long shell. These theories, however, are found to be inappropriate for the model employed here. This is mainly due to the relatively short length of the shell segment of the brake rotor. Thus, the following formulation resorts to the three-dimensional elasticity theory.

The derivation of the numerical procedure for modal analysis is based on the Hamilton's principle:

$$\delta H_c = \delta \int_{t_0}^{t_1} (T_c - E_c)\,\mathrm{d}t = 0 \tag{1}$$

in which, H_c denotes the Hamiltonian function defined as the integral of the difference of kinetic energy T_c and potential energy E_c of the system, provided the dynamic system is conservative. These energy terms,

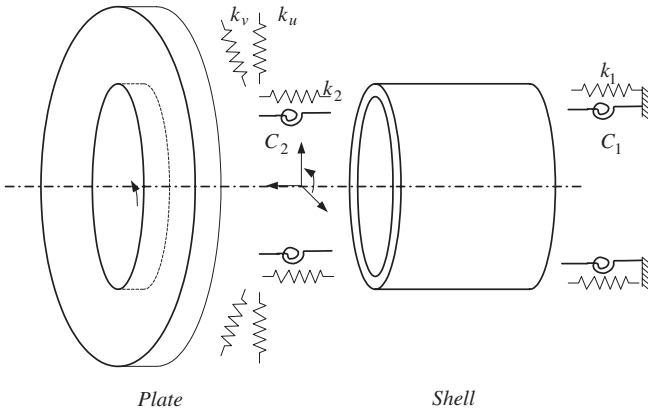

Fig. 1. Combined structure model of a disc brake rotor.

corresponding to the combined structure in Fig. 1, comprise the kinetic and elastic potential energies incurred by structural deformation of the plate and the shell segment, and the potential energy of the distributed artificial springs. Despite the apparent differences in their dimensions, both the annular plate and the shell segment can be regarded as a hollow cylindrical structure, complying with the general three-dimensional elasticity theory [15–17]. Therefore, energy analysis of a general hollow cylindrical structure is first derived, and then applied to the plate and shell part of the combined model. For this purpose, a cylindrical reference coordinate system (r, θ, x) is used as shown in Fig. 2. The figure also defines symbols to denote the dimensions of the hollow cylindrical structure.

Let u, v and w denote the displacement components in the direction of r, θ and x, respectively. According to the three-dimensional elasticity theory, the strain–displacement relationship with respect to the cylindrical coordinate system is expressed as

$$\varepsilon_{rr} = \frac{\partial u}{\partial r}, \quad \varepsilon_{\theta\theta} = \frac{1}{r}\frac{\partial v}{\partial \theta} + \frac{u}{r}, \quad \varepsilon_{xx} = \frac{\partial w}{\partial x},$$
$$\varepsilon_{r\theta} = \frac{1}{r}\frac{\partial u}{\partial \theta} + \frac{\partial v}{\partial r} - \frac{v}{r}, \quad \varepsilon_{rx} = \frac{\partial u}{\partial x} + \frac{\partial w}{\partial r}, \quad \varepsilon_{x\theta} = \frac{\partial v}{\partial x} + \frac{1}{r}\frac{\partial w}{\partial \theta}. \tag{2}$$

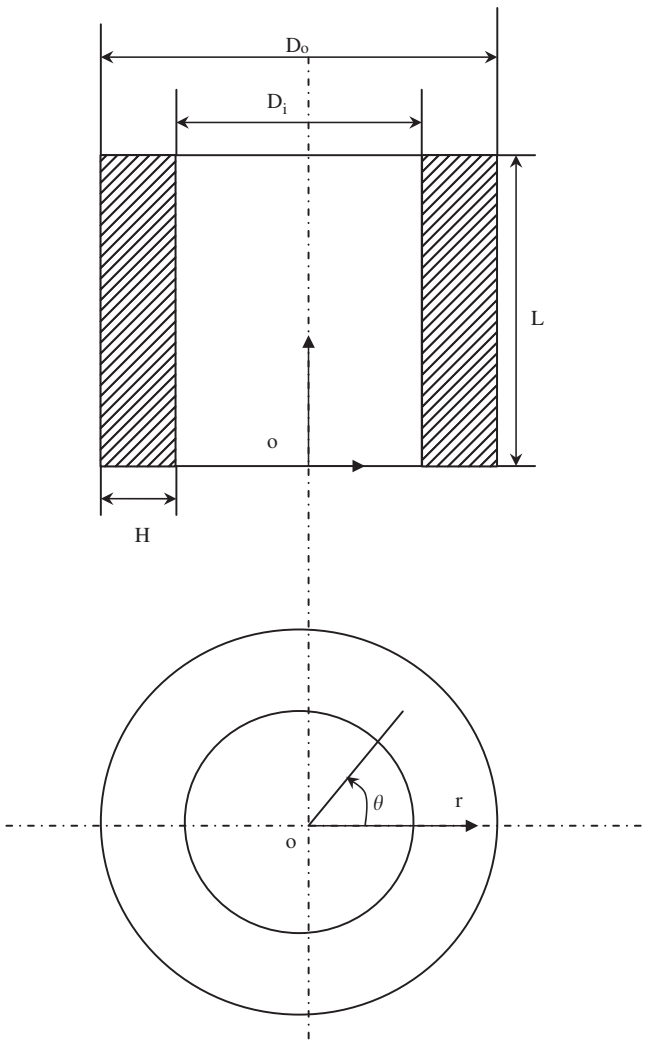

Fig. 2. General hollow cylindrical structures with corresponding reference coordinate system.

Translating the potential energy (E_c) and kinetic energy (T_c) into the functional of these displacement components with respect to the strain–stress and strain–displacement relationship yields

$$E_c = \frac{1}{2}\iiint \overline{E}\left\{(1-\mu)\left(\left(\frac{\partial u}{\partial r}\right)^2 + \frac{1}{r^2}\left(\frac{\partial v}{\partial \theta}+u\right)^2 + \left(\frac{\partial w}{\partial x}\right)^2\right) + 2\mu\left(\frac{1}{r}\left(\frac{\partial u}{\partial r}\right)\left(\frac{\partial v}{\partial \theta}+u\right) + \frac{1}{r}\left(\frac{\partial v}{\partial \theta}+u\right)\left(\frac{\partial w}{\partial x}\right) + \left(\frac{\partial u}{\partial r}\right)\left(\frac{\partial w}{\partial x}\right)\right) + \frac{(1-2\mu)}{2}\left(\left(\frac{1}{r}\frac{\partial u}{\partial \theta}+\frac{\partial v}{\partial r}-\frac{v}{r}\right)^2 + \left(\frac{\partial u}{\partial x}+\frac{\partial w}{\partial r}\right)^2 + \left(\frac{\partial v}{\partial x}+\frac{1}{r}\frac{\partial w}{\partial \theta}\right)^2\right)\right\} r\,\mathrm{d}r\,\mathrm{d}\theta\,\mathrm{d}x, \tag{3}$$

$$T_c = \frac{\rho}{2}\iiint (\dot{u}^2+\dot{v}^2+\dot{w}^2) r\,\mathrm{d}r\,\mathrm{d}\theta\,\mathrm{d}x, \tag{4}$$

where, $\overline{E} = E/(1+\mu)(1-2\mu)$ is a Lame constant; ρ the density; μ the Poisson's ratio and E the Young's modulus.

Different displacement components involved in the above expressions should then be expanded on the basis of a set of properly chosen admissible functions. It is proposed to adopt the trigonometric series for the circumferential expansion and the orthogonal polynomial series for the radial and axial expansions. Assuming harmonic response with an angular frequency ω, the expansion for these displacement components is expressed as:

$$u = \left\{f_u(r)g_u(x)\sum_n\sum_i\sum_j U_{ij}^n \phi_i(r)\varphi_j(x)\cos(n\theta)\right\}\mathrm{e}^{\mathrm{i}\omega t}, \tag{5}$$

$$v = \left\{f_v(r)g_v(x)\sum_n\sum_i\sum_j V_{ij}^n \phi_i(r)\varphi_j(x)\sin(n\theta)\right\}\mathrm{e}^{\mathrm{i}\omega t}, \tag{6}$$

$$w = \left\{f_w(r)g_w(x)\sum_n\sum_i\sum_j W_{ij}^n \phi_i(r)\varphi_j(x)\cos(n\theta)\right\}\mathrm{e}^{\mathrm{i}\omega t}, \tag{7}$$

in which, U_{ij}^n, V_{ij}^n and W_{ij}^n denote the expansion coefficients to be determined. $f_{[\cdot]}(r)$ and $g_{[\cdot]}(x)$ are incorporated here to satisfy the typical geometrical boundary conditions of the structure, which has been previously mentioned. These two functions are defined, respectively, as

$$f_{[\cdot]}(r) = \left(r-\tfrac{1}{2}D_i\right)^{\alpha_1^{[\cdot]}}\left(r-\tfrac{1}{2}D_o\right)^{\alpha_2^{[\cdot]}}, \tag{8}$$

$$g_{[\cdot]}(x) = x^{\beta_1^{[\cdot]}}(x-L)^{\beta_2^{[\cdot]}}, \tag{9}$$

where, D_i and D_0 are the internal and external diameters of the cylindrical structure, respectively, and L its length. In the above expressions, the exponents would be settled either as 0 or 1 depending on the boundary conditions. They are defined as follows:

For an annular plate: All exponents in Eq. (9), i.e. $\beta_1^{[\cdot]}$ and $\beta_2^{[\cdot]}$, are zeros, while exponents in Eq. (8) are defined as:

$$\alpha_{[i]}^{[u]} = 0, \alpha_{[i]}^{[v]} = 0, \alpha_{[i]}^{[w]} = 0, \quad i = 1, 2 : \text{for free circumferences;}$$
$$\alpha_{[i]}^{[u]} = 0, \alpha_{[i]}^{[v]} = 0, \alpha_{[i]}^{[w]} = 1, \quad i = 1, 2 : \text{for simply supported circumferences;}$$
$$\alpha_{[i]}^{[u]} = 1, \alpha_{[i]}^{[v]} = 1, \alpha_{[i]}^{[w]} = 2, \quad i = 1, 2 : \text{for clamped circumferences.}$$

For a cylindrical shell: All exponents in Eq. (8), i.e. $\alpha_1^{[\cdot]}$ and $\alpha_2^{[\cdot]}$, are zeros, while exponents in Eq. (9) are defined as:

$$\beta_{[i]}^{[u]} = 0, \beta_{[i]}^{[v]} = 0, \beta_{[i]}^{[w]} = 0, \quad i = 1, 2 : \text{for free circumferences;}$$
$$\beta_{[i]}^{[u]} = 0, \beta_{[i]}^{[v]} = 0, \beta_{[i]}^{[w]} = 1, \quad i = 1, 2 : \text{for simply supported circumferences;}$$
$$\beta_{[i]}^{[u]} = 1, \beta_{[i]}^{[v]} = 1, \beta_{[i]}^{[w]} = 2, \quad i = 1, 2 : \text{for clamped circumferences.}$$

In Eqs. (5)–(7), both $\{\phi_i(r)\}$ and $\{\varphi_j(x)\}$ are orthogonal polynomial series. Taking $\{\phi_i(r)\}$ as an example, the following shows the algorithms for its generation [18] with the initial conditions $\phi_0(r) = 0$ and $\phi_1(r) = 1$:

$$\phi_{i+1}(r) = (r - B_i)\phi_i(r) - C_i\phi_{i-1}(r), \quad i = 1, 2, 3, \ldots, \tag{10}$$

where

$$B_i = \int_c^1 r^2\phi_i^2(r)\,\mathrm{d}r \Big/ \int_c^1 r\phi_i^2(r)\,\mathrm{d}r$$

and

$$C_i = \int_c^1 r\phi_i^2(r)\,\mathrm{d}r \Big/ \int_c^1 r\phi_{i-1}^2(r)\,\mathrm{d}r,$$

where $c = D_i/D_o$. The potential energy contributed by the distributed artificial springs is expressed as

$$E_{kc} = \tfrac{1}{2}\int_{S_2}\int \left\{k_2(w_p - w_s)^2 + k_u(u_p - u_s)^2 + k_v(v_p - v_s)^2 + C_2\left(\frac{\partial w_p}{\partial r} + \frac{\partial u_s}{\partial x}\right)^2\right\} r\,\mathrm{d}r\,\mathrm{d}\theta$$
$$+ \tfrac{1}{2}\int_{S_1}\int \left\{k_1 w_s^2 + C_1\left(\frac{\partial u_s}{\partial x}\right)^2 + k_2(w_p - w_s)^2\right\} r\,\mathrm{d}r\,\mathrm{d}\theta \tag{11}$$

in which subscripts p and s refer to variables applied to the plate or to the shell of the combined structure, respectively. Substituting the expansion functions (5)–(7) and the energy expressions (3), (4) and (11) into the Hamiltonian function (1), extremization is performed using Lagrange's equation with respect to unknowns U_{ij}^n, V_{ij}^n, W_{ij}^n. A coupled linear equation in terms of all structural unknowns of the whole structure is finally obtained for a given circumferential expansion order n, which actually represents the number of the nodal diameters. Based on this linear equation, stiffness matrix and mass matrix can be formed and eigen analysis can be carried out. Modal solutions can then be obtained.

The convergence and accuracy of the model are first validated by applying the formulation to a free annular plate with a medium thickness. The benchmark plate is the one used by Leissa [15] with $H/D_o = 0.2$, $D_i/D_o = 0.5$ and $H = (D_o - D_i)/2$. The Poisson's ratio is $\nu = 0.3$. Table 1 tabulates results obtained by the present model and those extracted from Ref. [15], expressed in terms of the non-dimensional modal frequency Ω, which is defined as the ratio between the natural angular frequency and the wave velocity $\sqrt{4\overline{E}/\rho D_o^2}$. Calculations using the present model are carried out using different truncation orders for the polynomial series $\{\phi_i(r)\}$ and $\{\varphi_j(x)\}$. Note that Ω decreases when more terms are used, which is a well-known feature of the Rayleigh–Ritz method. Consistency and improved accuracy of the solution are evident, as the numbers of the expansion terms are gradually increased. Results presented hereafter use $(I, J) = (5, 3)$, $(7, 5)$ or $(9, 7)$ in different cases, with I, J being the maximum orders for $\{\phi_i(r)\}$ and $\{\varphi_j(x)\}$, respectively.

Table 1
Non-dimensional modal frequencies (Ω) of a plate with dimension $H/D_o = 0.2$, $D_i/D_o = 0.5$ and Poisson ratio $v = 0.3$

n	Ω (Symmetric modes)				Ω (Asymmetric modes)			
	Ref. [15]	$I = 5$ $J = 3$	$I = 7$ $J = 5$	$I = 9$ $J = 7$	Ref. [15]	$I = 5$ $J = 3$	$I = 7$ $J = 5$	$I = 9$ $J = 7$
0	2.234	2.234	2.234	2.233	1.388	1.391	1.388	1.388
	6.814	6.816	6.814	6.814	7.854	8.483	7.856	7.854
	9.957	10.209	9.958	9.957	8.321	8.660	8.323	8.321
	11.343	12.690	11.365	11.343	9.127	9.993	9.137	9.127
	12.207	12.904	12.228	12.207	10.398	11.021	10.399	10.398
	14.295	15.939	14.309	14.295	14.133	15.541	14.216	14.133
1	2.806	2.806	2.806	2.805	1.943	1.992	1.944	1.943
	7.372	7.378	7.372	7.372	8.039	8.481	8.041	8.039
	9.868	10.077	9.868	9.868	8.534	9.071	8.537	8.534
	11.386	12.697	11.408	11.386	8.945	9.744	8.953	8.945
	12.077	13.112	12.094	12.077	10.876	11.567	10.893	10.876
2	0.949	0.949	0.949	0.949	0.691	0.701	0.691	0.691
	4.177	4.178	4.177	4.177	3.123	3.241	3.124	3.123
	8.630	8.720	8.630	8.630	8.400	8.673	8.403	8.400
	9.721	9.956	9.722	9.721	8.793	9.508	8.800	8.793
	11.516	12.640	11.536	11.516	9.233	9.859	9.237	9.233
3	2.249	2.251	2.249	2.249	1.681	1.712	1.681	1.680
	5.717	5.719	5.717	5.717	4.450	4.635	4.451	4.450
	9.441	9.622	9.442	9.441	8.808	9.187	8.813	8.808
	10.270	11.048	10.271	10.270	8.986	9.577	8.991	8.986
	11.744	12.949	11.760	11.744	10.233	10.353	10.239	10.233
4	3.622	3.628	3.622	3.622	2.771	2.838	2.771	2.771
	7.209	7.216	7.209	7.209	5.805	6.057	5.807	5.805
	9.626	9.943	9.627	9.626	9.238	9.813	9.245	9.238
	11.310	11.790	11.315	11.310	9.587	9.834	9.593	9.587
	12.130	13.151	12.142	12.130	11.357	12.253	11.366	11.357

I and J are the maximum orders used in the expansion of the displacement components.

A full validation is conducted using a typical and complete disc brake rotor model. Dimensions of the annual plate are $D_i = 124\,\text{mm}$, $D_o = 237\,\text{mm}$, $L = 12\,\text{mm}$, and those of the shell segment are $D_i = 124\,\text{mm}$, $H = 5.5\,\text{mm}$ and $L = 23.5\,\text{mm}$. Two boundary conditions are considered for the shell at its right-hand side (see Fig. 1): free with $k_1 = 0$ and $C_1 = 0$; and supported with $k_1 = 3 \times 10^5\,\text{N/mm}$ and $C_1 = 5 \times 10^5\,\text{N/rad}$. The rigid connection between the shell and the plate is ensured using $k_u = 5 \times 10^9\,\text{N/mm}$, $k_v = 5 \times 10^9\,\text{N/mm}$, $k_2 = 5 \times 10^9\,\text{N/mm}$ and $C_2 = 5 \times 10^5\,\text{N/rad}$, all well exceeding the bending stiffness of the structure. It is pertinent to mention that, when the value of the spring stiffness is gradually increased, calculation results undergo a converging process. In simulating a rigid connection, the stiffness terms are gradually increased until no further variation is observed in terms of natural frequencies of the structure. More details on the selection of the spring stiffness can be found in Ref. [13]. Apart from the previously established formulation based on the three-dimensional elasticity theory, a parallel formulation using Mindlin plate theory and Flügge shell theory is also implemented to assess the applicability of these theories to the present configuration. FE simulation is conducted to provide reference solutions. The FE model uses three-dimensional eight-node elements, with each node having three translational degrees of freedom, to reconstruct the solid structure. The FE model involves a total of 16,288 nodes and 11,287 elements.

Table 2 compares the results obtained under the free boundary condition in terms of the non-dimensional modal frequency. Errors with respect to the FE results are calculated. The first several low-order modes for $n = 0$–6 are considered. The agreement between the present three-dimensional formulation and the FE results is obvious, with errors being mostly within 1–2%. Mindlin–Flügge theory apparently leads to much larger

Table 2
Non-dimensional modal frequencies (Ω) of the combined structure of brake rotor with free boundary conditions

n	FEM	Mindlin–Flügge theory		3D theory	
	Ω	Ω	Error (100%)	Ω	Error (100%)
0	0.3478	0.3003	13.68	0.3528	1.41
0	1.2079	1.2146	0.55	1.2089	0.09
0	1.7221	1.7819	3.48	1.7280	0.35
0	2.2308	2.1982	1.46	2.2371	0.28
1	0.5035	0.4513	10.37	0.5080	0.90
1	1.5126	1.5134	0.05	1.5115	0.08
1	1.6633	1.7459	4.97	1.6721	0.53
1	2.2480	2.2065	1.85	2.2506	0.12
2	0.1279	0.1224	4.25	0.1284	0.43
2	0.4544	0.4632	1.94	0.4532	0.26
2	0.8192	0.7670	6.38	0.8260	0.83
2	1.6998	1.7573	3.38	1.7069	0.42
3	0.3243	0.3143	3.10	0.3232	0.34
3	1.0077	1.0408	3.29	1.0094	0.17
3	1.1658	1.1396	2.25	1.1671	0.11
3	1.9487	1.9295	0.99	1.9477	0.05
4	0.5663	0.5522	2.49	0.5612	0.90
4	1.3119	1.4071	7.26	1.3170	0.39
4	1.7920	1.7394	2.93	1.7744	0.98
4	2.3081	2.2580	2.17	2.2985	0.41
5	0.8515	0.8304	2.48	0.8381	1.57
5	1.6203	1.7644	8.89	1.6120	0.51
6	1.1807	1.1466	2.89	1.1526	2.38
6	2.0043	2.1852	9.03	1.9704	1.69

errors, mainly due to the short length of the shell segment in the model. Similar comparison between the present three-dimensional formulation and FE simulation is performed for simply supported boundary as listed in Table 3. Similarly, typical errors totter around 1%, indicating a fairly good accuracy of the present approach.

3. Modal characteristics of the combined structure of the brake rotor

The following sections focus on the modal characteristics of the combined structure of the brake rotor model. We attempt to shed light on three aspects about the modal characteristics of the combined plate–shell structure: (a) mode classifications; (b) variations of modes with respect to the rotor dimensional parameters; (c) quantitative decomposition analysis of modes.

3.1. Mode classifications

There are a total of six displacement components (u_p v_p w_p and u_s v_s w_s), which account for the deformation of the combined structure for each mode. According to the relative deformation scale of these displacement components, the structure may exhibit various deformation patterns. The modes of the brake rotor are categorized according to these deformation patterns and ranked in an ascending order of the modal frequencies.

The three-dimensional mode shapes of the brake rotor are plotted in Fig. 3, corresponding to the modal results tabulated in Table 2. Generally speaking, the combined structure displays three typical deformation patterns. The structure might present overwhelming deformation only in its plate or shell part. Such type of modes is referred to as plate-dominant-mode (PDM) or shell-dominant-mode (SDM), respectively. For instance, Fig. 3 shows that all the first modes when $n = 2, 3, 4, 5, 6$ are PDMs, and all the second modes when $n = 3, 4, 5, 6$ are SDMs. By contrast, there exists also another category of modes, being referred to as strongly

Table 3
Non-dimensional modal frequencies (Ω) of the combined structure of brake rotor with supported boundary conditions

n	FEM	3D theory	
	Ω	Ω	Error (100%)
0	0.1930	0.1942	0.61
0	0.5809	0.5818	0.15
0	0.7082	0.6909	2.51
0	1.2092	1.2094	0.02
0	2.1792	2.1689	0.48
1	0.1731	0.1718	0.73
1	0.4910	0.4897	0.28
1	1.0101	1.0001	1.00
1	1.5143	1.5130	0.09
1	2.2515	2.2397	0.53
2	0.2362	0.2360	0.09
2	0.6114	0.6091	0.37
2	1.4480	1.4403	0.54
2	2.2482	2.2435	0.21
2	2.5081	2.4918	0.65
3	0.3879	0.3877	0.06
3	1.1523	1.1442	0.70
3	1.8413	1.8321	0.50
4	0.5948	0.5908	0.68
4	1.8293	1.8111	1.00
4	2.2018	2.1867	0.69
5	0.8626	0.8501	1.47
5	2.4988	2.4671	1.29
5	2.6151	2.5864	1.11

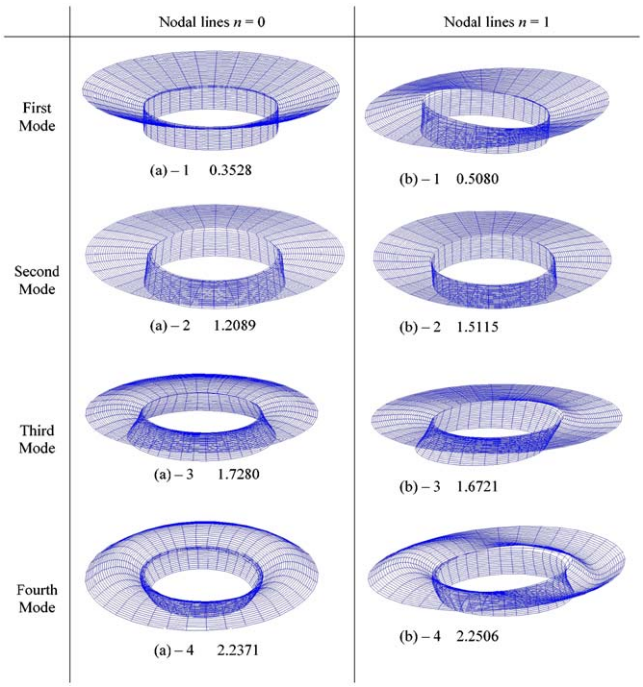

Fig. 3. Typical mode shapes of the brake rotor.

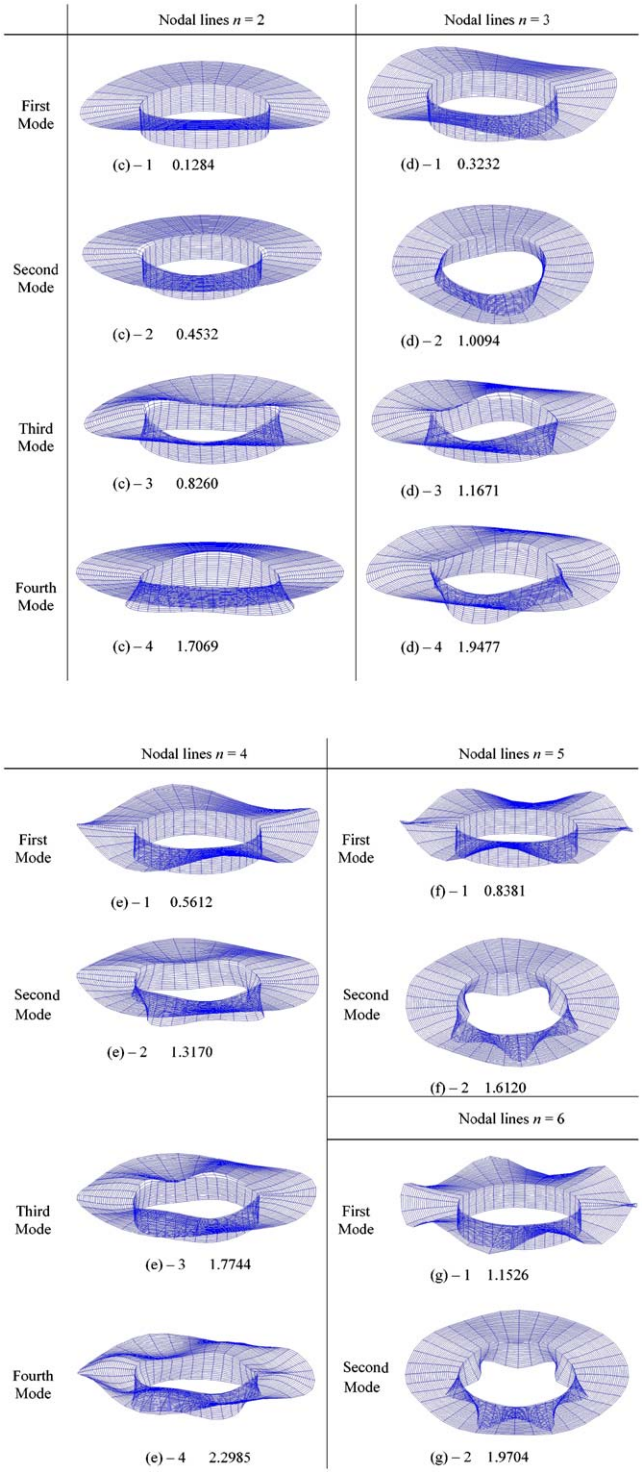

Fig. 3. (*Continued*)

coupled-mode (SCM), in which both the plate and shell of the combined structure exhibit strong deformations. Typical examples include the second and third modes when $n = 2$, and the third and fourth modes when $n = 3$.

Table 4
Classification of the combined structure modes, with PDM denoting plate-dominant-mode; SDM shell dominant mode and SCM strongly coupled-mode

	$n=0$	$n=1$	$n=2$	$n=3$	$n=4$	$n=5$	$n=6$
1st	PDM	SCM	PDM	PDM	PDM	PDM	PDM
2nd	PDM	PDM	SCM	SDM	SDM	SDM	SDM
3rd	SDM	SDM	SCM$^+$	SCM$^+$	SCM$^+$		
4th	SCM	SCM	SDM	SCM$^+$	SCM$^+$		

'$^+$' indicating strong deformation in w_p and v_p and/or v_s.

The differences in modal characteristics root in the way that structural coupling among the plate and shell takes place. An individual annular plate has well-separated in-plane (or longitudinal) and out-of-plane (or transversal) modes. An out-of-plane mode usually involves strong undulation (w_p) out of the flat surface of the plate. By contrast, an in-plane mode is primarily dominated by stretching and compression (u_p, v_p) within the plate surface. However, this simple classification is not suitable for a cylindrical shell due to its curved profile. The out-of-plane motion (w_s) and the in-plane motion (u_s and v_s) are interrelated for most of its modes. So does the incorporated model for the brake rotor. The mechanical joining in-between the plate and the shell destroys the decoupling between the in-plane and out-of-plane motions of the plate part. As inferred, transversal response of the plate is to be aroused to some extent, even though the combined structure is merely under an in-plane excitation, e.g. the tangential friction force. Such modes are most responsible for sound radiation. For this particular reason, attention should be paid to those modes in which the displacement components w_p and v_p and/or v_s are strong. Such deformation feature ensures that an in-plane force is able to excite the structure efficiently to generate a bending motion. These modes are marked by " $^+$" in Table 4.

Special attention is paid to the second modes whilst $n \geqslant 2$. In such modes, the plate of the combined structure shows nearly no out-of-plane motion but slight in-plane motion. By contrast, the shell presents obvious strong waveform along its circumference. Evidently, such modes would not be effective in making sound out of the combined structure.

3.2. Parametric study of modes

It is inferred that modes of the combined structure definitely have certain relationship with the modes of each substructure. How do the substructures interact to form the dynamic characteristics of the whole structure? How does such feature vary when dimensions of the combined structure change? To answer these questions, a parametric analysis is carried out. The analysis procedure is contrived to explain the association of the structure coupling with the combined structure modes, and also to reveal the influence of the structure dimensions and shape features on the dynamic characteristics of the combined structure.

The shell depth, which is one of the key parameters in the brake rotor design, is taken as variable and gradually changed from zero to a certain value, while the plate dimensions are fixed. Thus, as the shell depth changes, the whole structure would undergo continuous shape variations from an individual annular plate to a long shell fringed at one end with an annular plate.

Displayed in Fig. 4 are the modal characteristics of the tree typical combined structure modes varied with the shell depth. The shell depth is normalized to the external diameter of the plate using a non-dimensional relative shell depth defined as $L^* = L/D_o$. Particular attention is given to the low-frequency modes of the combined structure, which primarily relate to the low-frequency modes of the substructures, i.e. the plate and the shell. Such low-frequency modes have no nodal circles, whilst the number of nodal lines $n = 2, 3, 4$, respectively. The three selected modes of the combined structure involve the bending motion of the substructures. The bending magnitudes of the substructures are indicated by displacement components u_s and w_p, respectively. Two associated parameters are adopted to identify the characteristics of such modes. One is the previously defined non-dimensional modal frequency (Ω). The other is the bending magnitude ratio, defined as $\lambda^* = 10\log(\max(u_s)/\max(w_p))$, reflecting the bending deformation feature of the modes. The plate and shell display comparable bending magnitudes if λ^* is around zero. Large positive λ^* means the

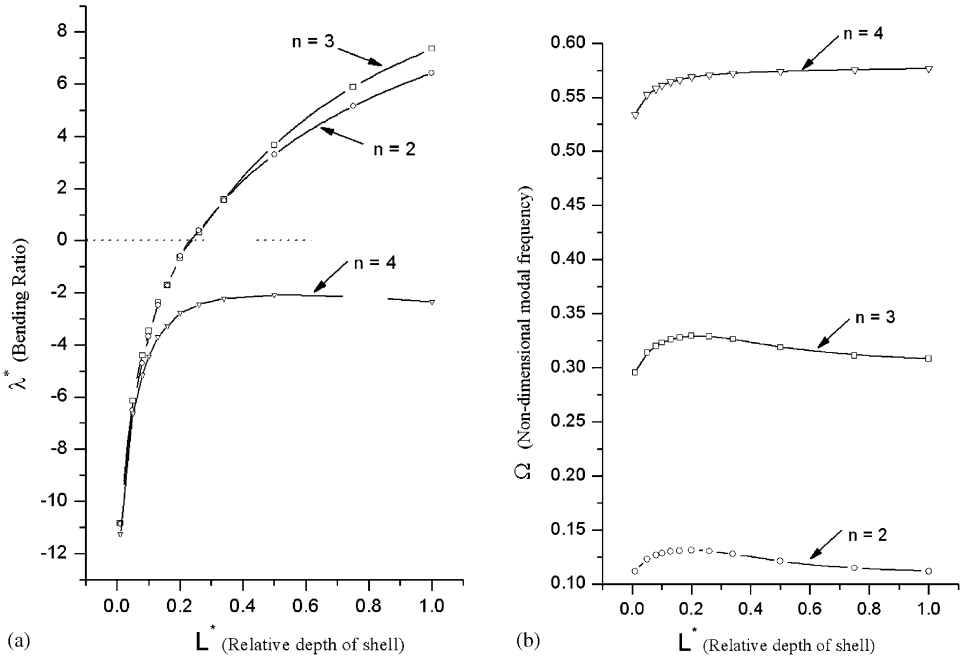

Fig. 4. Variation of modes with respect to the relative depth of the shell for $n = 2$, 3, 4 modes: (a) bending ratio λ^*; (b) non-dimensional modal frequency Ω.

overwhelming plate bending over that of the shell; otherwise, the opposite is true. The λ^*-L^* and $\Omega-L^*$ curves for the disc brake rotor are given in Figs. 4 (a) and (b) when $n = 2$, 3 and 4, respectively.

In Fig. 4(a), the climbing λ^*-L^* curves demonstrate the changes in the three mode shapes. A left downward extension of the λ^*-L^* curves implies a plate-bending dominant pattern of the deformation for all three modes, and the right upward extension implies a shell-bending dominant pattern for $n = 2$ and 3 modes. This implies that all three modes are dominated by plate bending while the shell is short. When the length of the shell increases, the shell reveals intensified bending motion for $n = 2$ and 3 modes. Strong coupling occurs at around $L^* = 0.2$ for these two modes. For $n = 4$ mode, however, plate domination is persistent through the entire region irrespective of the shell depth. The similarity between $n = 2$ and 3 modes and their difference with $n = 4$ mode are also reflected in Fig. 4(b). For the former, the $\Omega-L^*$ curves increase as the shell depth increases up to $L^* = 0.2$ before negotiating a smooth decrease. This is understandable since in the plate-dominant region ($L^* \ll 0.2$), the presence of the shell is to impose restrictions to the plate, such increasing its natural frequency, whilst in the shell-dominant region (($L^* \gg 0.2$), Ω decreases as the shell is getting longer, therefore more flexible. By contrast, $n = 4$ mode exhibits a stable Ω for large shell depth due to the dominance of the plate motion.

Modes of the combined structure and those of each substructure, before they are coupled together, are investigated with a view to shed light on their interrelationship. Fig. 5 shows the $\Omega-L^*$ curves of the first two modes when $n = 2$, for the combined structure (solid lines), plate (dot lines) and shell (dash lines). Since the dimensions of the plate are kept unchanged, the dot curves are just horizontal lines along L^*-axis. It can be seen that the first mode of the combined structure starts to deviate from the first mode of the plate when the depth of the shell is very short, before getting more close to the first mode of the shell when L^* increases. Note that the first mode of the shell involves a strong bending motion of the shell along its circumferential direction, whose stiffness increases with L^*. Apart from the reason given above to explain the increase of Ω at about $L^* = 0.2$, influence of the second mode of the shell at the peak region, corresponding to the intersection area between the membrane effect and bending effect, is also accountable. Variations of the second mode of the combined structure start from a plate mode (for small L^*), degenerate rapidly with an increasing L^*, and then evolve to a shell mode when L^* is large, basically following the variation of the second mode of the shell.

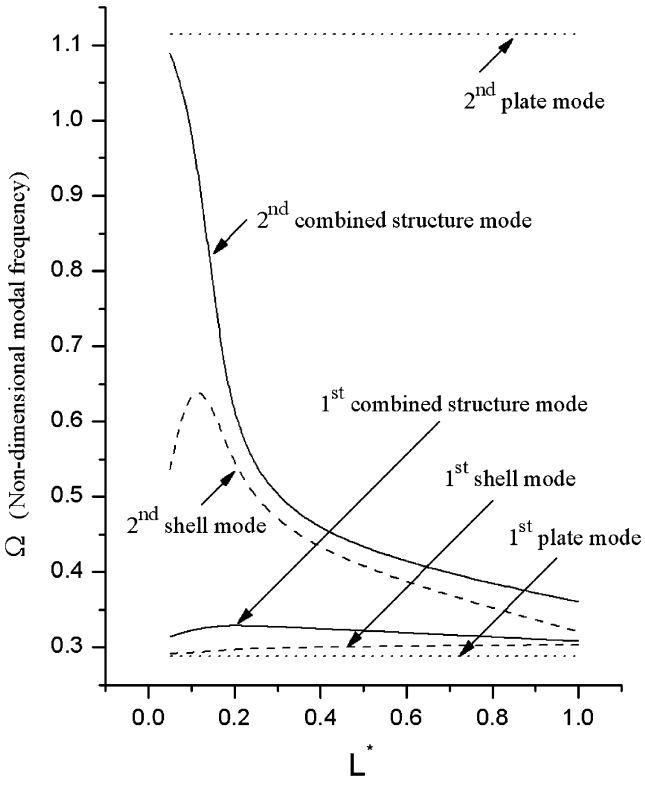

Fig. 5. Variation of the non-dimensional modal frequency Ω with respect to the relative depth of the shell for $n = 2$.

3.3. Decomposition analyses

As can be seen from the above discussion, one mode of the combined structure is either highly related to a certain plate or shell mode or a result of strong interaction among a number of substructure modes. Being able to quantify a given mode on the basis of sub-structural modes will be very helpful since the later can readily be obtained by simple structural analysis. To this end, a systematic procedure, being referred to as decomposition analysis, is proposed hereafter. Such decomposition helps to discern the modal characteristics of the combined structure through grasping the modal features of the substructure modes.

The general second-order differential vibration equation of the combined structure can be cast into the following general form for a given circumferential expansion order n:

$$-\omega^2\begin{bmatrix} M_p & \\ & M_s \end{bmatrix}\begin{Bmatrix} X_p \\ X_s \end{Bmatrix} + \begin{bmatrix} K_p & \\ & K_s \end{bmatrix}\begin{Bmatrix} X_p \\ X_s \end{Bmatrix} + \begin{bmatrix} K^c_{11} & K^c_{12} \\ K^c_{21} & K^c_{22} \end{bmatrix}\begin{Bmatrix} X_p \\ X_s \end{Bmatrix} = 0, \tag{12}$$

where $M_{[\cdot]}$ and $K_{[\cdot]}$ denote the mass and stiffness matrices of each substructure, respectively; $K^c_{[\cdot]}$ the connecting stiffness matrix due to the distributed artificial springs between the two substructures and $X_{[\cdot]}$ a vector containing all expansion coefficients (see Eqs. (5)–(7)). Subscript p (or s) applies to the plate (or shell).

Let $\Phi_{[\cdot]}$ and $\Lambda_{[\cdot]}$ be matrices containing the eigen solutions of the substructure and assume the following orthogonal relationships:

$$\begin{bmatrix} \Phi_p^{\mathrm{T}} & \\ & \Phi_s^{\mathrm{T}} \end{bmatrix}\begin{bmatrix} M_p & \\ & M_s \end{bmatrix}\begin{bmatrix} \Phi_p & \\ & \Phi_s \end{bmatrix} = \begin{bmatrix} I & \\ & I \end{bmatrix}, \tag{13}$$

$$\begin{bmatrix} \Phi_p^{\mathrm{T}} & \\ & \Phi_s^{\mathrm{T}} \end{bmatrix} \begin{bmatrix} K_p & \\ & K_s \end{bmatrix} \begin{bmatrix} \Phi_p & \\ & \Phi_s \end{bmatrix} = \begin{bmatrix} \Lambda_p & \\ & \Lambda_s \end{bmatrix}. \tag{14}$$

Let us define a new coordinate vector $\{q_p \quad q_s\}^{\mathrm{T}}$, which is the corresponding projection of the original unknown expansion coefficient vector $\{X_p \quad X_s\}^{\mathrm{T}}$ on the combined substructure modal space, i.e.

$$\begin{bmatrix} X_p \\ X_s \end{bmatrix} = \begin{bmatrix} \Phi_p & \\ & \Phi_s \end{bmatrix} \begin{bmatrix} q_p \\ q_s \end{bmatrix}. \tag{15}$$

A transformed Eq. (16) is obtained by substituting the projection relationship (15) into the original Eq. (12) and utilizing the modal transformation relationship among $\Phi_{[\cdot]}$, $M_{[\cdot]}$ and $K_{[\cdot]}$.

$$-\omega^2 \begin{Bmatrix} q_p \\ q_s \end{Bmatrix} + \begin{bmatrix} \Lambda_p & \\ & \Lambda_s \end{bmatrix} \begin{Bmatrix} q_p \\ q_s \end{Bmatrix} + \begin{bmatrix} \Phi_p^{\mathrm{T}} & \\ & \Phi_s^{\mathrm{T}} \end{bmatrix} \begin{bmatrix} K_{11}^c & K_{12}^c \\ K_{21}^c & K_{22}^c \end{bmatrix} \begin{bmatrix} \Phi_p & \\ & \Phi_s \end{bmatrix} \begin{Bmatrix} q_p \\ q_s \end{Bmatrix} = 0 \tag{16}$$

A subsequent eigen analsysis is to be conducted based on this equation, leading to eigen values and an eigen matrix. These eigen values give the modal frequencies of the combined structure and the eigen matrix is defined as the decomposition coefficient matrix. The ith row of this eigen matrix reflects how the ith mode of the combined structure is composed by the substructure modes, i.e. q_p nd q_s. Accordingly, the (i,j)th element of this matrix indicates how much the jth substructure mode contributes to the ith mode of the combined structure.

This decomposition analysis is conducted for the modes of the combined structure listed in Table 2. Results are given using bar-charts in Figs. 6(a)–(c). Selected modes include the first four modes whilst $n = 2, 3, 4$. The non-dimensional frequency of each mode is given in the horizontal axis. Distributed bars show decomposition coefficients of a given mode in terms of plate modes and shell modes, which are identified by "P" and "S", respectively, in the figures. Each group of the decomposition coefficients is normalized to the largest decomposition coefficient value within the group. Considering that the low-frequency modes of the combined structure are primarily composed of the low-frequency modes of the substructure, only the first five low-frequency modes of each substructure are included in the figures. The serial number following the symbol "P" or "S" indicates the order of the substructure mode in an increasing order of the modal frequency. Specifications about each mode of the substructure are tabulated in Table 5, so as to better understand the modal characteristics of the modes of the combined structure.

Using the bar-charts, one could (1) identify which individual substructure modes would dominate the mode of the combined structure, and (2) predict the deformation features of the combined structure. For example, for $n = 2$ mode ($\Omega = 0.1284$), Fig. 6(a) reveals that this mode is predominated by the first plate mode P1, which is an out-of-plane mode of the plate without nodal circles, as indicated in Table 5(a). S1 and S2 modes also contribute in a non-negligible manner. Referring to Table 5(a), superposition of S1 and S2 modes forecasts a bending motion of the shell part. For this mode, the plate part of the combined structure presents strong out-of-plane undulation; meanwhile, the circular profile of the shell moderately deforms into an oval shape. By contrast, the second $n = 2$ mode ($\Omega = 0.4532$) is mainly composed of P2 and S1. The former is an in-plane mode of the plate, while the latter demonstrates only bending with no longitudinal movement of the shell. Thus, the whole structure deforms only two dimensionally, without any undulation along the axial direction. Strongly coupled modes feature a strong contribution from several modes belonging to each substructure. Typical examples are the third and fourth modes when $n = 4$ ($\Omega = 1.7744$ and 2.2985 in Fig. 6(c)). Similar analysis also applies to all other modes, leading to conclusions consistent with the observations made in Fig. 3 and Table 4.

4. Conclusions

Most existing analytical studies on the brake rotor dynamics simplify the brake rotor as a thin annular plate. Such simplification neglects inherent structural coupling of the brake rotor, such warranting the development of more realistic models, along with necessary analysis tools. The primary objective of this paper

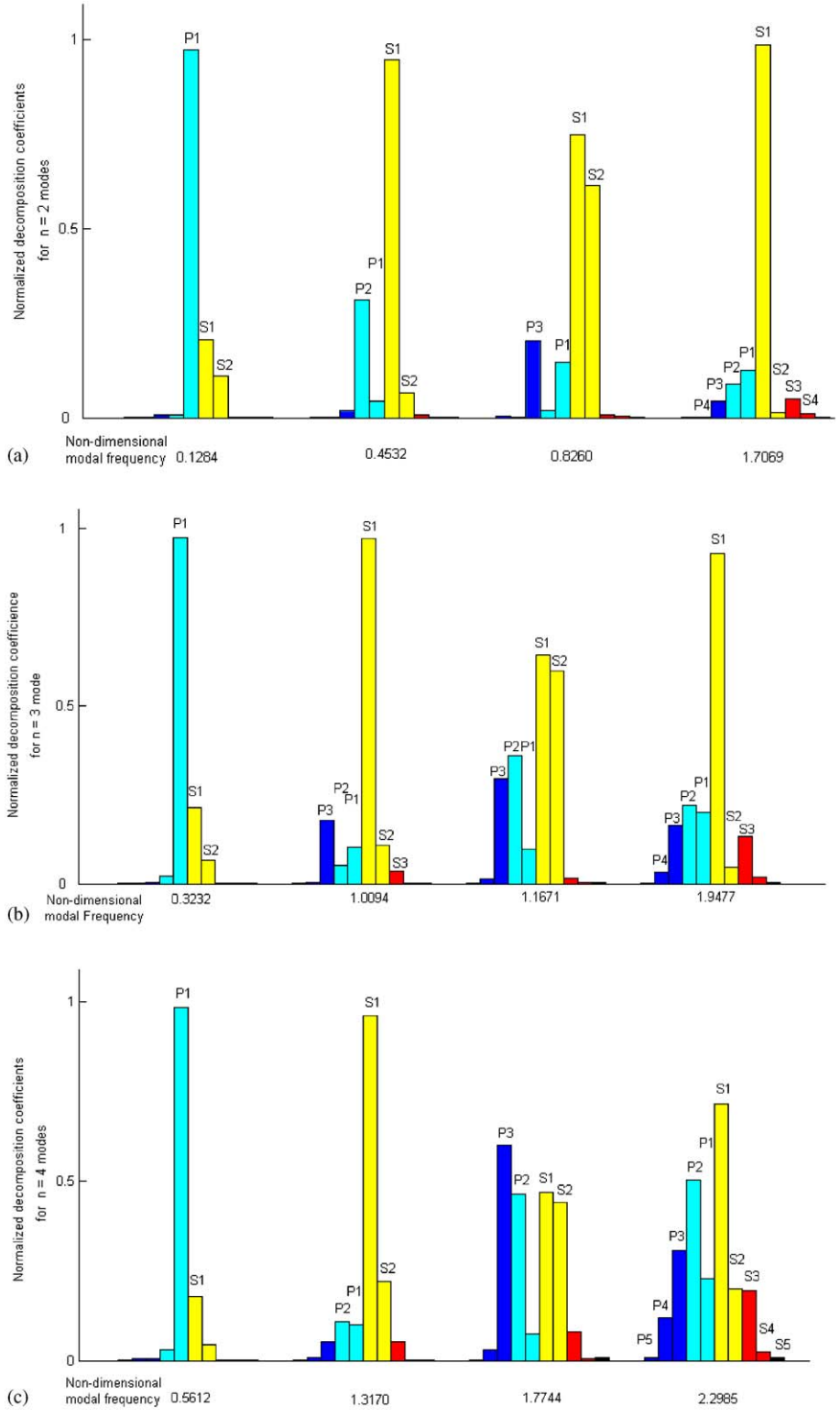

Fig. 6. Decomposition bar-charts for the modes of the combined structure: (a) $n = 2$; (b) $n = 3$; (c) $n = 4$.

Table 5
Modal characteristics of the substructure modes used in Fig. 6(a)–(c)

Serial no.	Plate mode (P)	Shell mode (S)
(a) with $n = 2$		
1	Out-of-plane (0, 2)	Bending without longitudinal motion
2	In-plane (0, 2)	Bending plus longitudinal motion, without nodal circle
3	Out-of-plane (1, 2)	Bending plus longitudinal motion, with one nodal circle
4	In-plane (1, 2)	Torsional motion
(b) with $n = 3$		
1	Out-of-plane (0, 3)	Bending without longitudinal motion
2	In-plane (0, 3)	Bending plus longitudinal motion, without nodal circle
3	Out-of-plane (1, 3)	Bending plus longitudinal motion, with one nodal circle
4	Out-of-plane (2, 3)	Torsional motion
(c) with $n = 4$		
1	Out-of-plane (0, 4)	Bending without longitudinal motion
2	Out-of-plane (1, 4)	Bending plus longitudinal motion, without nodal circle
3	In-plane (0, 4)	Bending plus longitudinal motion, with one nodal circle
4	Out-of-plane (2, 4)	Torsional motion

(m, n) stands for the number of nodal circles and nodal diameters, respectively.

is to propose such a model and subsequently to study its modal characteristics, which is believed to be useful in further investigation on the noise in automotive disk brake system.

The proposed brake rotor model is a combination of an annular plate and a cylindrical shell segment connected together by distributed artificial springs. The model presents two main appealing features: one is its closeness to a real brake rotor in terms of structural complexity; the other one is the facility it offers to carry out dynamic analyses using a semi-analytical approach. Based on a three-dimensional elasticity theory, a numerical procedure is established using variational principle and Raleigh–Ritz method.

Numerical simulations are performed. Modal solutions are found to agree well with FE results. Modal analyses show the existence of three types of modes for the combined structure, which can be classified as PDM, SDM and SCM, depending on the involvement of each substructure. From the squeal noise control point of view, those modes, demonstrating strong coupling between w_p and v_p/v_s, should be targeted. Such deformation feature ensures the efficiency of an in-plane force in exciting the structural vibration with dominant bending motion, which is responsible for sound generation.

A decomposition technique is proposed. The technique allows each mode of the combined structure to be translated into a linear combination of the individual substructure modes. It is shown that the decomposition coefficients provide a practical means to carry out mode classifications and systematically quantify the complex deformation features of the modes.

Reference

[1] R. Spurr, A theory of brake squeal, *Proceedings of the Institution of Mechanical Engineers* 1 (1961–1962) 33–40.
[2] K.B. Dunlap, M. A. Riehle, R. E. Longhouse. An investigation overview of automotive disc brake noise. *SAE Paper* 1999-01-0142. 1999.
[3] N.M. Kinkaid, O.M. O'Reilly, P. Papadopoulos, Review: automotive disc brake squeal, *Journal of Sound and Vibration* 267 (2003) 105–166.
[4] M.L. Chargin, L.W. Dunne, D.N. Herting, Nonlinear dynamics of brake squeal, *Finite Elements in Analysis and Design* 28 (1997) 69–82.
[5] D.H. Guan, J.C. Huang, The method of feed-in energy on disc brake squeal, *Journal of Sound and Vibration* 261 (2003) 297–307.
[6] H. Ouyang, J.E. Mottershead, W. Li, A moving-load model for disc-brake stability analysis, *Journal of Vibration and Acoustics* 125 (2003) 53–58.

[7] H. Ouyang, J.E. Mottershead, M.P. Cartmell, D.J. Brookfield, Friction-induced vibration of an elastic slider on a vibrating disc, *International Jounal of Mechanical Sciences* 41 (1999) 325–336.
[8] J. Hultén, J. Flint, An assumed modes method approach to disc brake squeal analysis, *SAE Paper* 1999-01-1335, 1999.
[9] J. Flint, J. Hultén, Lining-deformation-induced modal coupling as squeal generator in a distributed parameter disc brake model, *Journal of Sound and Vibration* 254 (2002) 1–21.
[10] F. Chen, S. E. Chen, P. Harwood, In-plane mode/friction process and their contribution to disc brake squeal at high frequency, *SAE Paper* 2000-01-2773, 2000.
[11] M. Yang, A. H. Afaneh, P. Blaschke, A study of disc brake high frequency squeals and disc in-plane/out-of-plane modes, *SAE Paper* 2003-01-1621, 2003.
[12] J.C. Bae, J.A. Wickert, Free vibration of coupled disk-hat structures, *Journal of Sound and Vibration* 235 (2000) 117–132.
[13] L. Cheng, J. Nicolas, Free vibration analysis of cylindrical shell-circular plate system with general coulping and various boundary conditions, *Journal of Sound and Vibration* 155 (1992) 231–247.
[14] J. Yuan, S.M. Dickinson, The free vibration of circularly cylindrical shell and plate systems, *Journal of Sound and Vibration* 175 (1994) 241–263.
[15] J. So, A.W. Leissa, Three dimensional vibrations of thick circular and annular plates, *Journal of Sound and Vibration* 209 (1998) 15–41.
[16] J. So, A.W. Leissa, Free vibrations of thick hollow circular cylinders from three-dimensional analysis, *Journal of Sound and Vibration* 119 (1997) 89–95.
[17] D. Zhou, F.T.K. Au, Y.K. Cheung, S.H. Lo, Three-dimensional vibration analysis of circular and annular plates via the Chebyshev-Ritz method, *International Journal of Solids and Structures* 40 (2003) 3089–3105.
[18] C.S. Kim, S.M. Dickinson, On the lateral vibration of thin annular and circular composite plates subject to certain compliance effects, *Journal of Sound and Vibration* 130 (1989) 363–377.